PAPER

Check for updates

Red and NIR active dipod–SDS self-assemblies for "turn on" quantification of spermine in serum, urine and food: smart-phone assisted on-site determination of spermine in amine-rich foods†

Nancy Singla, [iD] *[a] Sukhvinder Dhiman, [iD] [a] Manzoor Ahmad, [iD] [a] Satwinderjeet Kaur,[b] Prabhpreet Singh [iD] [a] and Subodh Kumar [iD] *[a]

Spermine is a vital biomarker for clinical diagnosis of cancer and estimating food spoilage. Here, supramolecular assemblies of two donor–π–acceptor dipods R-SPM (λ_{em} 640 nm) and NIR-SPM (λ_{em} 720 nm) with SDS have been discovered for the detection of spermine and spermidine under physiological conditions at nanomolar levels. The addition of SDS to R-SPM and NIR-SPM results in the formation of self-assemblies (DLS, zeta-potential and UV-vis studies) with no significant change in their fluorescence but further addition of spermine/spermidine to the R-SPM∩SDS and NIR-SPM∩SDS assemblies results in a 30–80 fold increase in fluorescence intensity, respectively at 640 nm and 720 nm. The LOD for spermine and spermidine detection is 22 nM (4.4 ppb) and 67 nM (9.7 ppb). The ensembles show nominal interference from other biogenic amines, amino acids, metal ions, and anions. Both R-SPM∩SDS and NIR-SPM∩SDS ensembles can be stored in the dark for >3 months without affecting their performance. The potential of these ensembles for real world applications like analysis of spermine in urine, human serum and food spoilage in the case of cheese, mushrooms, chicken and mutton has been demonstrated. The smartphone relied RGB analysis facilitates the on-site determination of spermine in food samples.

1. Introduction

Spermine (SPM) and spermidine (SPD) are vital biomarkers in clinical diagnosis of cancer and estimating food spoilage in the food industry. SPM and SPD exert multiple functions in many physiological and pathophysiological processes, including cell proliferation, differentiation, growth, tissue regeneration and gene regulation. The concentration of spermine ranges from 1 to 40 μM in blood,[1] 59 to 233 μM in serum,[2] and 100 to 400 nM in urine[3] depending upon age and gender.[4] The alteration in their concentrations in urine or blood can be taken as indicators of malfunctioning in living systems. Spermidine concentrations are markedly decreased with age[5] and in persons having Alzheimer's disease.[6] Long-term oral intake of polyamine-rich diet causes an increase in blood polyamine levels and delays the onset of Alzheimer's disease. In cancer patients, the levels of spermine

in blood samples increase by 3 to 5-fold compared with those found in healthy people.[7–9] Therefore, a high level of polyamines is regarded as a biomarker for the timely diagnosis of cancer in certain tumors.[7–9]

Spermine is present in most meat products like sausages, pork, chicken, and turkey, some vegetables like pumpkin, and also in cheese. Spermidine is present in a large number of foods like dry soy bean, chicken liver, green peas, corn, shell fish, and blue cheese.[10] Although these do not have any adverse effect, during cooking, SPM/SPD may react with nitrite to form carcinogenic nitrosamines in meat products that contain nitrite and nitrate salts as curing agents.[11,12] A fresh food consists of very low levels of amines, whereas, after fermentation, their concentrations are elevated.[13] Thus it becomes imperative to develop methods that can detect spermine and spermidine in biofluids and food samples with high selectivity and sensitivity especially in a very small volume of sample.

Cucurbit[n]urils (CB[n], n = 5–8, 10, 14) are effective in encapsulating and solubilizing hydrophobic organic molecules by weak non-covalent interactions. Fluorescent dyes complexed with a nanoparticle, quantum dot or cyclodextrin exhibit reversal in its fluorescence response on addition of cucurbituril (CB) *via* host–guest complexation.

[a] Department of Chemistry, Centre for Advanced Studies, Guru Nanak Dev University, Amritsar, Punjab, India. E-mail: nancy38452@gmail.com
[b] Department of Botanical and Environment Sciences, Guru Nanak Dev University, Amritsar, India

The addition of spermine to this assembly then again changes the fluorescence response. Thus either the off–on–off[14–16] or on–off–on[17] phenomenon has been used for SPM and SPD detection. In a two component process, a fluorescent dye forms a host–guest complex with metals such as Tb^{3+},[18] Cu^{2+},[19–21] Ag^+,[22,23] Au^{3+},[24,25] Fe^{3+} (ref. 26), etc. via non covalent interactions. This complex is then dissociated with spermine and spermidine due to their higher affinity towards metals. DNA capped metal nanoparticles[27–29] have also been used for spermine and spermidine detection. Triphenylethylene based fluorescent dyes with terminal sulphate or carboxylate groups[30–33] form electrostatic complexes with SPM and SPD and result in fluorescence enhancement due to restriction in rotation.

However, most of the reported methods are based on fluorescence quenching with SPM /SPD or emission enhancement in the blue or green region (Table 1). The supramolecular assemblies of CB or SDS with fluorescent probes have shown promise to achieve better selectivity by the displacement approach or by binding of SPD/SPM with the negatively charged amphiphiles. There is only one report where the self-assembly of a dye with CB on interaction with SPD/SPM gives fluorescence enhancement in the NIR region (730 nm) (entry 4, Table 1) but it has not found practical applications.

In present investigations, supramolecular assemblies of two donor–π–acceptor dipods R-SPM (λ_{em} 640 nm) and NIR-SPM (λ_{em} 720 nm) with SDS have been explored for the detection of SPM and SPD. R-SPM∩SDS and NIR-SPM∩SDS ensembles result in 30–80 fold increase in fluorescence intensity respectively at 640 nm and 720 nm on addition of 10 equivalents of SPM and SPD. The LOD for SPM and SPD detection is 22 nM (4.4 ppb) and 67 nM (9.7 ppb). These

assemblies show nominal interference from other biogenic amines, amino acids, metal ions and inorganic anions. These assemblies can be stored in the dark for >3 months without affecting their performance. The potential of these ensembles for real world applications like analysis of spermine from urine, human serum and food spoilage in the case of cheese, mushroom, chicken and mutton has been demonstrated. The smartphone trusted RGB analysis speeds up the detection for real-time analysis of spermine.

2. Experimental

2.1 Synthesis of R-SPM

In 25 ml RBF, 1,2-bis(bromomethyl)benzene 1 (132 mg, 0.5 mmol) and (E)-N,N-dimethyl-4-(2-(pyridin-4-yl)vinyl)aniline (224 mg, 1 mmol) were dissolved in acetonitrile (15 ml) and the reaction mixture was refluxed with continuous stirring at 90 °C for 16 h. After completion of the reaction, the precipitates were filtered, washed with a diethyl ether and chloroform (1 : 1) mixture and dried to get red precipitates, 326 mg, yield 92%, melting point 254 °C; ^1H NMR (DMSO-d_6, 400 MHz, ppm): δ 2.98 (s, 12H, 4× NCH_3), 5.87 (s, 4H, 2× NCH_2), 6.69 (d, J = 8.8 Hz, 4H, ArH), 7.12 (d, J = 16 Hz, 2H, 2× olefin H), 7.25–7.28 (m, 2H, ArH), 7.49–7.51 (m, 2H, ArH), 7.52 (d, J = 8.8 Hz, 2H, ArH), 7.88 (d, J = 16 Hz, 2H, 2× alkene H), 8.00 (d, J = 6.8 Hz, 4H, ArH), 8.64 (d, J = 6.8 Hz, 4H, ArH); ^{13}C NMR (DMSO-d_6, 100 MHz, ppm): δ 24.4, 58.4, 111.4, 116.4, 121.9, 122.1, 129.6, 130.0, 132.6, 142.6, 143.1, 149.9, 152.6, 153.9; HRMS: mol. formulae $C_{38}H_{40}Br_2N_4$, exact mass expected 710.162; $C_{38}H_{40}BrN_4^+$ 631.2431, 633.2410; $C_{38}H_{40}N_4^{2+}$ 552.3242/2 = 276.1621, obtained for $C_{38}H_{40}BrN_4^+$ at m/z 631.2275, 633.2271; $C_{38}H_{40}N_4^{2+}$ at 276.1533 (M).

Table 1 Comparison of performance with some recent reports on fluorescence-based systems for the detection of spermine

Sr. no.	Emission maxima	Solvent system	FL ON/OFF	LOD	Application in urine	Application in serum	Application in food	Smartphone determination	Ref.
1.	640 nm, 720 nm	99.9% HEPES buffer	"On"	22–34 nM	YES	YES	YES	YES	This work
2.	425 nm	HEPES buffer–DMSO (95 : 5)	"Off"	6 nM 500 nM	YES	YES	NO	NO	3c
3.	535 nm	Water	"Off"	0.5 nM-SP 6 nM-SPD	YES	YES	NO	NO	14
4.	735 nm	Water	"On"	99 nM-SP 179 nM-SPD	NO	NO	NO	NO	14
5.	615 nm	Water	"Off"	70 nM-SP 330 nM-SPD	YES	YES	YES	NO	15
6.	475 nm	Water	"Off"	14 nM-SP 36 nM-SPD	YES	YES	NO	NO	16
7.	556 nm	HEPES buffer–CH_3CN (1 : 1)	"Off"	0.09 nM	YES	YES	YES	NO	20
8.	493 nm	HEPES buffer–CH_3CN (3 : 7)	"Off"	600 nM	YES	NO	YES	NO	21
9.	562 nm	HEPES buffer–CH_3CN (1 : 1)	"On"	27.5 nM	YES	YES	NO	NO	37
10.	415 nm	Aqueous solution	"Off"	330 nM	YES	NO	NO	NO	38
11.	570 nm, 450 nm	Aqueous solution	"Off"	200 nM-SP 2100 nM-SPD	NO	NO	YES	NO	39
12.	380–550 nm	Water	"On"	6000 nM	YES	YES	NO	NO	40

© 2024 The Author(s). Published by the Royal Society of Chemistry

2.2 Synthesis of NIR-SPM

1,2-Bis(bromomethyl)benzene (132 mg, 0.5 mmol) and diene **8** (250 mg, 1 mmol) were dissolved in acetonitrile (5 ml) and the reaction mixture was refluxed with continuous stirring at 90 °C for 16 h. The solid separated was filtered, washed with diethyl ether and dried. Red coloured precipitates of **NIR-SPM** were obtained, 513 mg, 85% yield, melting point 231 °C. ^{1}H NMR (500 MHz, DMSO-d$_6$): δ 2.99 (s, 12H, 4× CH$_3$), 5.95 (s, 4H, 2× NCH$_2$), 6.66 (d, J = 8.8 Hz, 4H, ArH), 6.69 (d, J = 16 Hz, 2H, alkene H), 7.01–7.07 (m, 4H, ArH), 7.21–7.33 (m, 2H, ArH), 7.38 (d, J = 8.8 Hz, 4H, ArH), 7.49–7.52 (m, 2H, ArH), 7.78 (dd, J_1 = 16 Hz, J_2 = 10 Hz, 2H, alkene H, ArH), 7.98 (d, J = 7.2 Hz, 4H, ArH), 8.70 (d, J = 7.2 Hz, 4H, ArH); ^{13}C NMR (125 MHz, DMSO-d$_6$): δ 59.3, 112.5, 123.4, 123.6, 123.9, 129.7, 130.6, 130.7, 133.3, 143.4, 144.1, 144.9, 151.6, 154.3; HRMS: mol. formulae C$_{42}$H$_{44}$Br$_2$N$_4$ exact mass expected for C$_{42}$H$_{44}$-BrN$_4^+$ = 683.2744, 685.2723 (1 : 1), C$_{42}$H$_{44}$N$_4^{2+}$ = 604.2968/2 = 302.1778, obtained 683.2073, 685.2060 (1 : 1); 302.1484.

2.3 Preparation of solutions

The stock solutions of fluorescent probes **R-SPM** and **NIR-SPM** (1 mM) were prepared in DMSO and were further diluted for preparing solutions of desired concentrations. For the preparation of 10 μM solution, 100 μL of stock solution was taken into a 10 ml volumetric flask and filled up to the mark with desired solvent like a DMSO–HEPES mixture or HEPES buffer. Typically, freshly prepared stock solutions of spermine and spermidine were prepared in deionized water. All the proteins, enzymes, amino acids and anions were prepared by dissolving commercial reagents in Millipore double distilled water.

2.4 Quantitative detection of spermine in urine using R-SPM∩SDS and NIR-SPM∩SDS ensembles

The quantitative detection of spermine using the fluorescence approach was carried out by collecting the fresh, morning urine of a healthy female donor. The urine collected was filtered with a 0.02 μm syringe microfilter to remove any suspended particle. To remove the protein present, 3 ml of urine sample was mixed with 70 μl of 70% perchloric acid. This mixture was then centrifuged at 7000 rpm for 35 min and then placed at room temperature for 15 min. The supernatant fluid obtained was again filtered through a 0.02 μm filter and adjusted to neutral pH with sodium hydroxide. The urine (1000 μl) was added to 2000 μl of **R-SPM∩SDS** (15 μM∩750 μM) or **NIR-SPM∩SDS** (15 μM∩750 μM) ensemble. The final concentration of the probe and SDS was 10 and 500 μM. Finally, the concentration of spermine in the urine sample was detected by recording the fluorescence spectra of these solutions. The amount of spermine present was evaluated from the calibration curve obtained by titrating **R-SPM∩SDS** (10 μM∩500 μM) and **NIR-SPM∩SDS** (10 μM∩500 μM) ensembles with spermine under standard conditions.

2.5 Quantitative detection of spermine in human serum using R SPM∩SDS and NIR-SPM∩SDS ensembles

The human blood serum of a healthy female donor was collected from the pharmacy department of our university and stored at −20 °C. The serum samples were centrifuged at 7000 rpm for 15 min, maintaining the temperature between 15 and 20 degrees Celsius. The supernatant liquid was collected and for 1 mL of the supernatant, 3 mL of acetone was added to precipitate the proteins and it was again centrifuged at 7000 rpm for 35 min maintaining the low temperature. After that, the supernatant was collected and was used for the quantification of spermine in serum. The processed human serum sample (200 μl) was added to 3 ml of **R-SPM∩SDS** (10 μM∩500 μM) or **NIR-SPM∩SDS** (10 μM∩500 μM) ensemble and fluorescence spectra were recorded.

2.6 Quantitative detection of spermine in food samples using R SPM∩SDS and NIR-SPM∩SDS ensembles

Fresh samples of two vegetarian food: mushroom and cheese as well as two non-vegetarian food: chicken and mutton were obtained from a local market and were stored at 20 degrees Celsius. These were (5 g each) placed in separate 50 ml glass beakers having 20 ml of water. The experiments were performed in triplicate. The **R-SPM∩SDS** (12 μM∩600 μM) or **NIR-SPM∩SDS** (12 μM∩600 μM) ensemble (2.5 ml) was treated with 500 μl of water for each food sample solution and the fluorescence spectra of resulting 3 ml solutions were recorded to determine the quantity of spermine released. For the next 3 days, 500 μl of water from each food sample was taken and their fluorescence spectra were recorded to determine the quantity of spermine released.

3. Results and discussion

3.1 Synthesis and characterization of R-SPM and NIR-SPM

The stirring of 4-methylpyridine (**1**) with benzoyl chloride (**2**) in DMF within 30 minutes *in situ* generated the 4-methylpyridinium moiety (**3**) which remains in equilibrium with the enamine (**4**). The enamine (**4**) on condensation with 4-dimethylaminobenzaldehyde (**5**) gave mono-ene derivative **6** in 54% yield. Similarly, enamine (**4**) on condensation with 4-dimethylaminocinnamaldehyde (**7**) gave diene **8** in 30% yield (Scheme S1†).

The reaction of 1,2-bis(bromomethyl)benzene (**9**) with two equivalents of mono-ene **6** in acetonitrile at reflux temperature gave **R-SPM**, in 92% yield (Scheme 1). The presence of two 2H doublets with J = 16 Hz at δ 7.12 and δ 7.88 in the ^{1}H NMR spectrum of **R-SPM**, and its exact mass for C$_{38}$H$_{40}$N$_4^{2+}$ at 276.1693 (M/2) confirm the formation of **R-SPM**. Similarly, the reaction of 1,2-bis(bromomethyl)benzene (**9**) with two equivalents of diene **8** in acetonitrile at reflux temperature gave **NIR-SPM**, in yield 85% (Scheme 1). The presence of a NCH$_2$ singlet of four protons at δ 5.95 ppm in its ^{1}H NMR spectrum and its exact mass for C$_{42}$H$_{44}$N$_4^{2+}$ at 302.1484 (M/2) confirm the formation of **NIR-SPM** (Fig. S1–S6†).
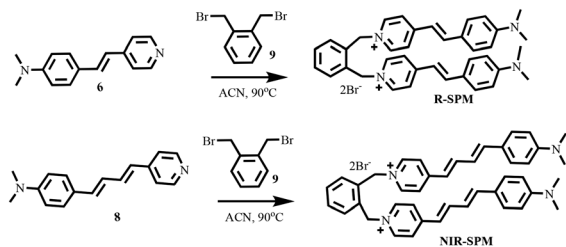
Scheme 1 Synthesis of **R-SPM** and **NIR-SPM**.

3.2 Effect of water on UV-vis and florescence spectra of R-SPM and NIR-SPM in DMSO–water binary mixtures

The UV-vis and fluorescence spectra of **R-SPM** and **NIR-SPM** in DMSO–water (HEPES buffer pH 7.4) binary mixtures provide vital information about their molecularly dissolved or aggregate state under different aqueous conditions and thus provide vital information for further design of experiments.

The UV-vis spectrum of **R-SPM** in DMSO gives an absorption band at 490 nm which on gradual increase in amount of HEPES buffer is blue shifted and in 99.9% buffer appears at 474 nm (Fig. S7A and B†). The molar absorptivity of the solutions remains quite stable at 64500 ± 2500 L mol^{-1} cm^{-1}. The probe **R-SPM** in DMSO, on excitation at 490 nm, gives an emission spectrum with maximum at 640 nm. The fluorescence colour of the solution appears red. On gradually increasing the fraction of water (HEPES buffer, pH 7.4) in DMSO–water binary mixtures, the fluorescence intensity at 640 nm sequentially decreases sharply up to 50% of water fraction and on further increasing the fraction of water from 60% to 99.9%, the fluorescence is slowly decreased (Fig. S7C,† 1D). The quantum yield in DMSO is found to be 1.78%, which is reduced to 0.81% in 99.9% buffer. The dynamic light scattering experiments reveal that the probe **R-SPM** in DMSO–water (buffer) binary mixtures remains as mono-dispersed aggregates (Fig. S7,† E1–E4). The hydrodynamic diameter of these aggregates gradually decreases with an increase in fraction of water (buffer). In 20% buffer, the hydrodynamic diameter of aggregates is 181 nm, which decreases to 130, 27 and 25 nm on respective increases in fraction of water to 40%, 80% and 99.9%.

The UV-vis spectrum of **NIR-SPM** (10 μM) in DMSO gives an absorption band with maxima at ~510 nm ($\varepsilon = 75\,900$ L mol^{-1} cm^{-1}) (Fig. S8A,† 2B). The steady addition of water amount to **NIR-SPM** solution in DMSO results in gradual blue shift in the absorption maximum and is associated with a decrease in the absorption. In 99.9% buffer, the absorption maximum is blue shifted by 30 nm to 480 nm in comparison to that in DMSO and the ε value is decreased to 54 500 L mol^{-1} cm^{-1}. This blue-shift in absorption maximum is attributed to the H-aggregation of the molecules of **NIR-SPM** with the increase in fraction of water.

The probe **NIR-SPM** in DMSO on excitation at 490 nm gives an emission spectrum with maximum at 740 nm (Fig. S8C†). The addition of water results in a fast decrease in

fluorescence intensity at 740 nm (Fig. S8D†) and in the DMSO–buffer (1:1) mixture, the fluorescence intensity is reduced by >90%. Further increase in f_w shows a nominal decrease in fluorescence intensity. The quantum yield in DMSO is found to be 6.26%, which is reduced to 0.84% in 99.9% buffer. The dynamic light scattering experiments reveal that in 40% buffer (Fig. S8,† E1), **NIR-SPM** exists as nano-aggregates with a hydrodynamic diameter of 232 nm. The size of aggregates is reduced to 94 and 23 nm on increasing the fraction of HEPES buffer to 60% and 80%. In 99.9% buffer, **NIR-SPM** exists as aggregates with a diameter of 50 nm. Therefore, both **R-SPM** and **NIR-SPM** with increasing amounts of water undergo aggregation induced fluorescence quenching, though this quenching is more efficient up to 50% water fraction.

3.3 Effect of SDS on UV-vis and fluorescence spectra of R-SPM and NIR-SPM

R-SPM (10 μM, HEPES buffer, 0.1% DMSO) gives an absorption spectrum with maximum at 470 nm. On addition of SDS, the absorbance at 470 nm gradually decreases up to addition of 80 μM SDS. On further increasing the concentration of SDS, a new absorbance band appears at 530 nm (Fig. 1A) and achieves a plateau on addition of 200 μM SDS (Fig. 1B). On excitation at 490 nm, the emission spectrum exhibits weak emission with maximum at 640 nm, the intensity of which gradually increases with the increase in concentration of SDS (Fig. 1C). After addition of 500 μM SDS, a nearly six times increase in emission intensity is observed.

NIR-SPM (10 μM) in HEPES buffer exhibits an absorbance spectrum with maximum at 480 nm. On addition of SDS up to 50 μM, the maximum does not undergo any change. However, on further addition of amounts of SDS the maximum undergoes gradual red-shift (Fig. 1D) and on addition of 300 μM SDS, the absorbance shifts to 512 nm
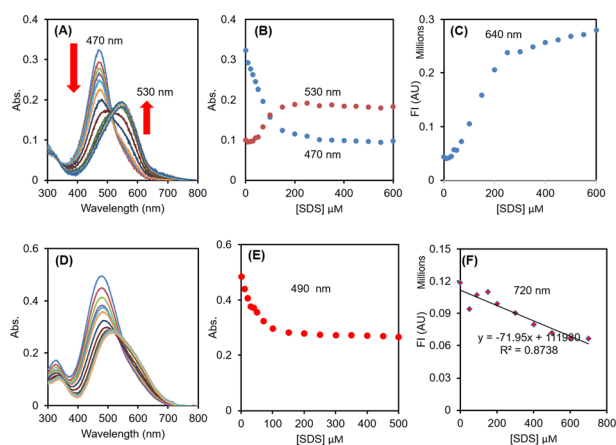

Fig. 1 Effect of SDS on UV-vis and fluorescence spectra (A–C) = **R-SPM**; (D–F) = **NIR-SPM**; (A and D) effect of SDS on the UV-vis spectrum; (B and E) plot of [SDS] *vs.* absorbance; (C and F) effect of [SDS] on fluorescence intensity.

and then becomes stable. The plot of absorbance at 490 nm against [SDS] shows a steady decrease in absorbance with addition of SDS up to 150 μM and then achieves a plateau (Fig. 1E). During this process, the molar absorbance of **NIR-SPM** is decreased from 46 700 L mol^{-1} cm^{-1} to 27 800 L mol^{-1} cm^{-1}. On excitation at 490 nm, **NIR-SPM** gives weak fluorescence with maximum at 720 nm, which steadily decreases to half of its value with 500 μM SDS (Fig. 1F). This decrease in fluorescence intensity is in agreement with the decrease in absorbance.

Therefore, for probes **R-SPM** and **NIR-SPM**, the effect of SDS on their UV-vis spectra is similar but in the case of fluorescence studies, the fluorescence intensity of **R-SPM** exhibits a 6-fold increase while **NIR-SPM** shows a small decrease.

3.4 Selectivity of R-SPM∩SDS and NIR-SPM∩SDS towards spermine and spermidine

To rationalize the effect of SDS concentration on the sensitivity of **R-SPM∩SDS** and **NIR-SPM∩SDS** ensembles towards SPM and SPD, the solutions of **R-SPM** (10 μM) and **NIR-SPM** (10 μM) were treated with 100 μM spermine and then were titrated with SDS. The fluorescence spectrum of **R-SPM** and **NIR-SPM** remained unaffected by the addition of spermine. On steady addition of SDS to these solutions, the fluorescence intensity gradually increased (Fig. S9†). Both probes showed a maximum increase in fluorescence intensity with 500–600 μM SDS. Therefore, for all further studies for evaluation of **R-SPM** and **NIR-SPM** towards various species, the respective self-assemblies were prepared by treating 10 μM probe with 500 μM SDS.

We have evaluated the selectivity of **R-SPM∩SDS** and **NIR-SPM∩SDS** assemblies towards spermine and spermidine in comparison to various biological amines, thiols, amino acids and proteins. In each case, 5 equivalents of the target species was added to **R-SPM∩SDS** and **NIR-SPM∩SDS** and the fluorescence spectra were recorded using 490 nm excitation wavelength. **R-SPM∩SDS** with spermine and spermidine exhibited respective 17-fold and 8-fold increase in

fluorescence intensity at 640 nm, whereas the addition of other amines, amino acids, thiols, proteins, *etc.* did not exhibit any observable change in fluorescence intensity of the **R-SPM∩SDS** ensemble (Fig. S10†). The solutions of **R-SPM∩SDS** with spermine and spermidine appeared red under 365 nm light, whereas the solutions containing other analytes remained non-fluorescent.

Similarly, **NIR-SPM∩SDS** with spermine and spermidine exhibited respective 48-fold and 18-fold increase in fluorescence intensity at 720 nm, whereas the addition of other amines, amino acids, thiols, proteins, *etc.* did not cause any observable change in fluorescence intensity of **NIR-SPM∩SDS** (Fig. 2A and B). The solutions of **NIR-SPM∩SDS** with spermine and spermidine appeared red under 365 nm light, whereas the solutions containing other analytes remained non-fluorescent. The solution **NIR-SPM∩SDS** having HSA, the most abundant protein in plasma, exhibited weak fluorescence with a blue-shifted emission band at 680 nm.

Therefore, both **R-SPM∩SDS** and **NIR-SPM∩SDS** ensembles exhibit a sharp increase in fluorescence intensity with spermine and spermidine and remain silent to other analytes and can find application for the detection of spermine and spermidine. These results are in contrast to earlier reported results, where dipod∩**SDS** ensembles resulted in fluorescence quenching with spermine.[3c]

3.5 Quantitative detection and sensitivity of R-SPM∩SDS and NIR-SPM∩SDS towards spermine and spermidine

The UV-vis spectrum of **R-SPM∩SDS** (10∩500 μM, HEPES buffer) exhibited an absorption maximum at 490 nm. On gradual addition of spermine, the absorbance of the **RSPM∩SDS** ensemble marginally increased and was associated with red-shift of the maximum to 540 nm (Fig. 3A and B). However, addition of spermidine to **R-SPM∩SDS** resulted in the red-shift in the absorbance band and was associated with minimal change in absorbance (Fig. 3C and D).

The UV-vis spectrum of **NIR-SPM∩SDS** (10∩500 μM, HEPES buffer) gave an absorption band with maxima at ~510 nm (ε =
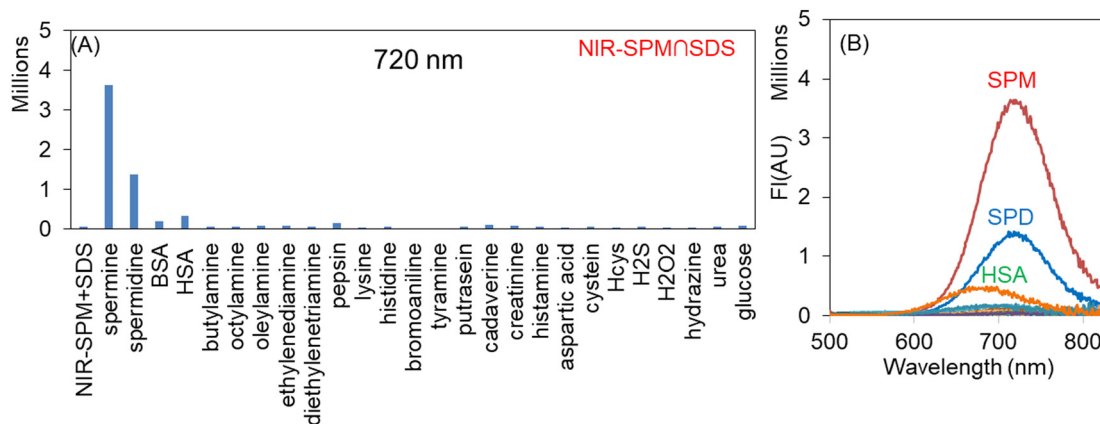

Fig. 2 (A) The bar diagrams showing the change in fluorescence intensity on addition of 5 equivalents each of different species to NIR-SPM∩SDS (10–500 μM, HEPES buffer). (B) The fluorescence spectra of **NIR-SPM∩SDS** in the presence of different analytes.
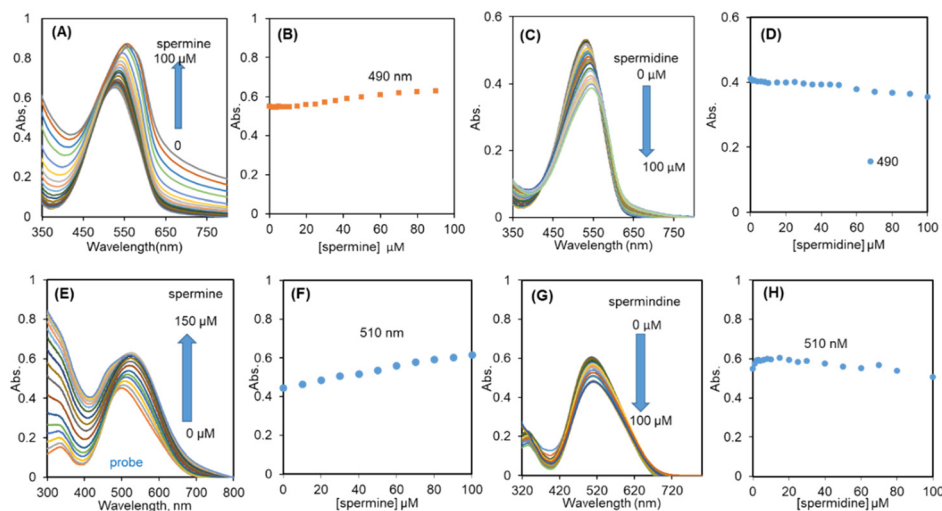
Fig. 3 The effect of spermine and spermidine on the UV-vis spectrum of (A and C) R-SPM∩SDS (10∩500 μM, HEPES buffer) and (E and G) NIR-SPM∩SDS (10∩500 μM, HEPES buffer) ensembles; (B and D) plot of absorbance on addition of (B) spermine; (D) spermidine in R-SPM∩SDS solution; (F and H) plot of absorbance on addition of (F) spermine; (H) spermidine in NIR-SPM∩SDS solution.

$48\,600$ L mol^{-1} cm^{-1}) (Fig. 3E). The gradual addition of spermine resulted in ~10 nm red-shift in absorption maximum and an increase in the ε value to $61\,700$ L mol^{-1} cm^{-1} up to 100 μM spermine, beyond which only a residual increase was observed (Fig. 3F). The tail of the absorbance band extended to longer wavelength *i.e.* beyond 800 nm in the case of interaction of spermine with R-SPM∩SDS or NIR-SPM∩SDS and led to the formation of bigger aggregates and increased Mie scattering of the respective solutions. However, interaction of spermidine with the R-SPM∩SDS or NIR-SPM∩SDS ensemble resulted in minimal lowering in absorbance with only a small increase in Mie scattering and so the size of aggregates (Fig. 3G and H).

The UV-vis studies have been well supported by DLS experiments. The probe R-SPM (10 μM, HEPES buffer) exists as aggregates with 25 nm size. On addition of SDS, the average size of aggregates of R-SPM∩SDS (10 μM, 500 μM) was increased to ~40 nm. The addition of spermine (100 μM) to R-SPM∩SDS (10 μM, 500 μM) resulted in the increase in size of aggregates to 217 (62%) and 591 nm (37%). This increase in size of aggregates could result in the increased Mie scattering observed in UV-vis experiments (Fig. 4, left column). However, the addition of spermidine (100 μM) to R-SPM∩SDS (10 μM, 500 μM) formed aggregates with only 180 nm size and caused Mie scattering to a small extent only. The probe NIR-SPM (10 μM, HEPES buffer) in buffer exists as nano-aggregates of 50 nm size. On addition of SDS (500 μM) the size of aggregates was increased to 58 nm size (98%) and 238 nm (2%). The addition of spermine (100 μM) to NIR-SPM∩SDS aggregates led to increased size of aggregates to 240 nm (40%) and 585 nm (60%) and was associated with Mie scattering in UV-vis experiments (Fig. 4, right column). The spermidine (100 μM) formed NIR-SPM∩SDS∩spermidine ensembles with an average size of 240 nm. Therefore, spermine with both R-SPM∩SDS and NIR-SPM∩SDS formed larger (~590 nm) aggregates than those formed by spermidine (~200 nm).

Further to rationalize the step-wise interaction of aggregates with SDS and then with spermine and spermidine, zeta potential studies were performed. The probe R-SPM shows a zeta potential of −2.7 mV which points to the strong electrostatic interactions of bromide ions on the surface of aggregates. The zeta potential of aggregates of R-SPM on interaction with SDS goes to a further negative value of −13.7 mV pointing to the presence of negatively charged SDS molecules on the surface of R-SPM aggregates. The spermine interacts on the surface of these aggregates resulting in a lower negative zeta potential of −7.1 mV pointing to partial neutralization of effect of SDS molecules. However, due to the interaction of aggregates of R-SPM with SDS and then with spermine, the size of aggregates is substantially
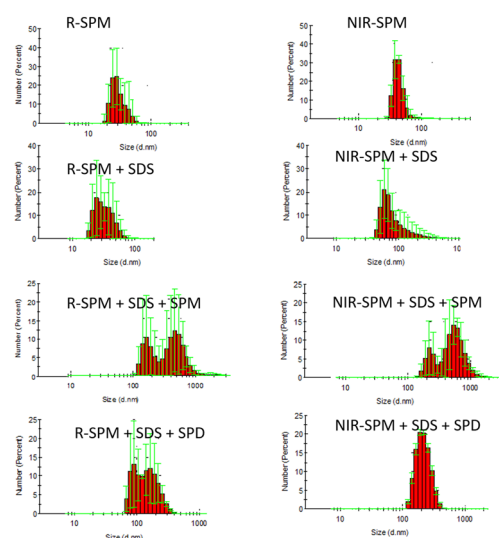

Fig. 4 The DLS studies showing the effect of SDS, spermine and spermidine on the size of aggregates of R-SPM (left column) and NIR-SPM (right column).

increased (DLS studies, Fig. 4). The spermidine molecules interact at a lesser extent on the surface of **R-SPM∩SDS** aggregates and cause a smaller change in zeta potential to −11.0 mV. **NIR-SPM** exhibits similar results with SDS, followed by spermine and spermidine. The zeta potential of **NIR-SPM** aggregates is −0.8 mV which on interaction with SDS reaches −13.7 mV and on further interaction with spermine is shifted to −7.7 mV.

The fluorescence lifetime studies of **NIR-SPM** showed that it fits in the biexponential curve. The fluorescence lifetime τ_1 remained constant at around 0.1 ns after addition of SDS and spermine. However, on addition of SDS to **NIR-SPM**, τ_2 showed a decrease in its value from 27.43 ns to 23.95 ns. Here, the aggregates of **NIR-SPM** loosen up and electron transfer from SDS sulfonate to the pyridinium moiety keeps the low fluorescence. The addition of spermine to these aggregates resulted in the decrease in lifetime to 14.84 ns in the presence of 10 equivalents of spermine. The change in the lifetime values shows that the mechanism is dynamic. The decrease in the lifetime strongly supports the participation of a photoinduced electron transfer process.[34] The strong electrostatic interactions between quaternary salt of spermine and sulfonate of SDS inhibit the PET from sulfonate of SDS to pyridinium moieties. This results in an increase in fluorescence after addition of spermine to **NIR-SPM–SDS** solution (Scheme 2). A similar phenomenon results in enhanced fluorescence of **R-SPM–SDS** solution on interaction with spermine.

On addition of aliquots of spermine to **R-SPM∩SDS** (10∩500 μM, HEPES buffer), a steady increase in the fluorescence intensity at 640 nm was observed up to addition of 70 μM spermine. Further addition of spermine resulted in only a residual increase in the fluorescence intensity (Fig. 5A and B). **R-SPM∩SDS** with spermine (100 μM) resulted in a ~29-fold increase in fluorescence intensity and appeared red under 365 nm light. The fluorescence increased linearly between 0 μM and 70 μM spermine and could detect as low as 22 nM spermine (Fig. 5C). However, titration of **R-SPM∩SDS** with spermidine (100 μM) resulted in a 16-fold increase in fluorescence intensity at 640 nm, after which only a residual increase was observed (Fig. 5D and E). The

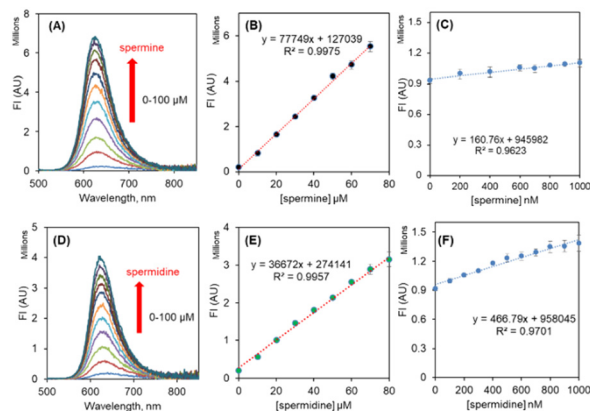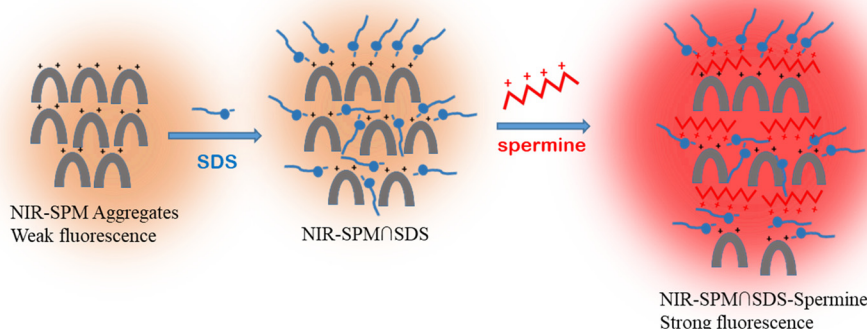**Fig. 5** (A) Fluorescence spectra of **R-SPM∩SDS** (10∩500 μM) with incremental addition of spermine; (B) plot of the fluorescence intensity *vs.* [spermine] at 640 nm in μM concentration range slit 2/2; (C) plot of the fluorescence intensity *vs.* [spermine] at 640 nm in nM concentration range slit 4/4; (D) fluorescence spectra of **R-SPM∩SDS** (10∩SDS μM) with incremental addition of spermidine; (E) plot of the fluorescence intensity *vs.* [spermidine] at 640 nm in μM concentration range slit 2/2; (F) plot of the fluorescence intensity *vs.* [spermidine] at 640 nm in nM concentration range slit 4/4.

R-SPM∩SDS ensemble can detect spermidine with an LOD of 77 nM (Fig. 5F).

NIR-SPM∩SDS (10∩500 μM, HEPES buffer) with spermine exhibited a steady increase in the fluorescence intensity at 720 nm up to addition of 60 μM spermine. Further addition of spermine resulted in only a residual increase in the fluorescence intensity (Fig. 6A and B). **NIR-SPM∩SDS** with spermine (100 μM) resulted in a ~80-fold increase in fluorescence intensity and appeared red under 365 nm light. The fluorescence increased linearly between 0 and 1000 nM spermine and could detect as low as 34 nM spermine (Fig. 6C). However, titration of **NIR-SPM∩SDS** with spermidine (100 μM) resulted in a 29-fold increase in fluorescence intensity at 720 nm, after which only a residual increase was observed (Fig. 6D and E). The **NIR-SPM∩SDS** ensemble can detect spermidine with an LOD of 67 nM (Fig. 6F). The LOD values have been calculated as per IUPAC norms.

Scheme 2 Schematic representation of the mechanism involved in selective sensing of spermine by **R-SPM∩SDS** and **NIR-SPM∩SDS** ensembles.
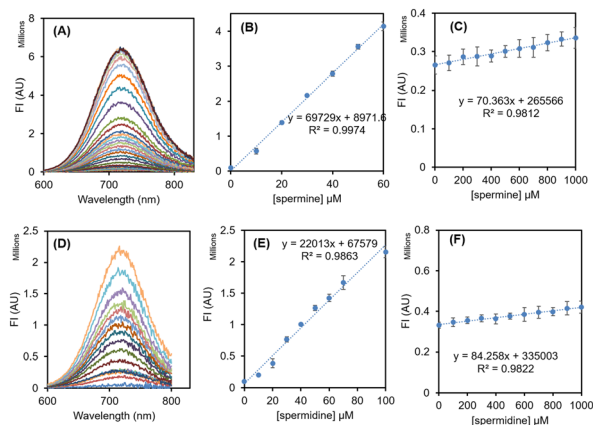
Fig. 6 (A) Fluorescence spectra of **NIR-SPM∩SDS** (10∩500 μM) with incremental addition of spermine; (B) plot of the fluorescence intensity *vs.* [spermine] at 720 nm in μM concentration range slit 3/3; (C) plot of the fluorescence intensity *vs.* [spermine] at 720 nm in nM concentration range slit 5/5; (D) fluorescence spectra of **NIR-SPM∩SDS** (10∩SDS μM) with incremental addition of spermidine; (E) plot of the fluorescence intensity *vs.* [spermidine] at 720 nm in μM concentration range slit 3/3; (F) the plot of the fluorescence intensity *vs.* [spermidine] at 720 nm in nM concentration range slit 5/5.

3.6 Effect of temperature on fluorescence intensity of ensembles and on interaction of ensembles with spermine

In order to rationalize the effect of temperature on the fluorescence intensity of **R-SPM∩SDS**, **NIR-SPM∩SDS**, **R-SPM∩SDS∩spermine** and **NIR-SPM∩SDS∩spermine**, the respective solutions were heated from 20 to 60 °C and then were allowed to cool back to 20 °C and the fluorescence spectra were recorded with every 5 °C change in temperature.

NIR-SPM∩SDS revealed a minimal effect of temperature on its fluorescence intensity between 20–60 °C. The **R-SPM∩SDS**, **R-SPM∩SDS∩spermine** and **NIR-SPM∩SDS∩spermine** ensembles exhibited a gradual decrease in fluorescence intensity with an increase in temperature but on lowering the temperature, the fluorescence intensity reverted back to the initial value. The decrease in fluorescence intensity on increasing temperature could be assigned to the increase in flexibility in ensembles leading to faster decay of excited states. The reversibility of fluorescence intensity on variation in temperature clearly shows their equilibration by controlling temperature (Fig. 7).

3.7 Analysis of spermine in biofluids like urine and serum

For real time or practical application of the developed ensembles, real biological samples of human urine and human blood serum were collected as their collection is non-invasive, easily available and also they have biomarkers whose concentration variations can cause various types of cancer in the human body. We firstly studied the interference of various components present in urine such as sodium and potassium salts, urea, uric acid, creatinine and proteins *viz.* BSA and HSA. It was found that the proteins at 1 μM concentration resulted in
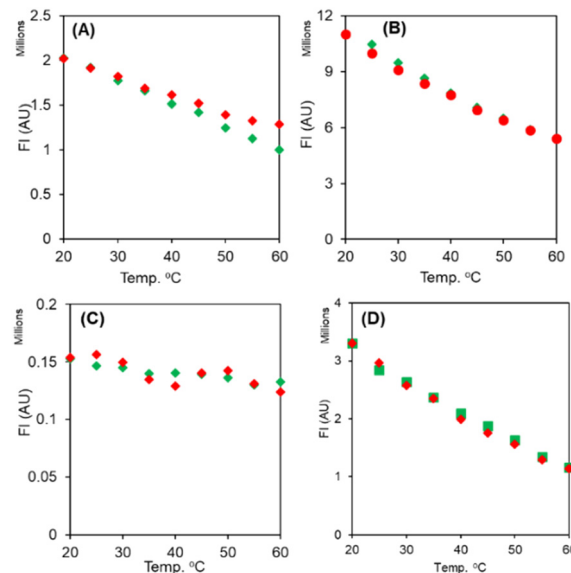

Fig. 7 Effect of temperature on fluorescence intensity of (A) **R-SPM∩SDS** (10∩500 μM, HEPES buffer); (B) **R-SPM∩SDS∩spermine** (10∩500∩100 μM, HEPES buffer); (C) **NIR-SPM∩SDS** (10∩500 μM, HEPES buffer); (D) **NIR-SPM∩SDS∩spermine** (10∩500∩100 μM, HEPES buffer).

<1% enhancement in the fluorescence signal with a blue shift, whereas other species do not induce any change in fluorescence even when present at 50 μM amounts. We analyzed urine samples taken from two healthy subjects. The pretreated urine sample (1000 μl) was added to the solution of **R-SPM∩SDS** (15 μM∩750 μM) and **NIR-SPM∩SDS** (15 μM∩750 μM) and the fluorescence values were compared to the standard calibration curve after taking three replicate measurements. In the urine samples, spermine was found to be 376 ± 75 nM and 297 ± 91 nM which are in agreement with most of the reported values of spermine in healthy human urine.[3]

The pretreated serum sample (200 μl) was added to **R-SPM∩SDS** (10 μM∩500 μM)/**NIR-SPM∩SDS** (10 μM∩500 μM) and their fluorescence spectra were recorded. The fluorescence intensities were compared to the standard calibration curve after taking three replicate measurements. In the serum sample, spermine was found to be 225 ± 48 μM and 112 ± 31 μM which are in the range of reported values of spermine in healthy human blood serum.[2]

3.8 Quantitative determination of spermine in four different food samples

For evaluation of real time application of the probes∩**SDS** complex, four types of food items having rich amounts of spermine were chosen. These foods are degraded by enzymes by various routes like amine oxidase, copper-containing amine oxidase or xanthamine oxidase. Also, the uncontrolled microbial enzymatic action results in aggregation of biogenic amines which degrade food products.[35] These microorganisms are mainly active at high storage temperatures, high pH and under aerobic conditions.

5.0 grams of each food sample was dipped in 20 ml of double distilled water and stored at 4 °C and 35 °C. Each time 500 μl of water from these samples was taken and was added to **NIR∩SDS** (12 μM∩600 μM) (2.5 ml) solution to keep the final concentration of **NIR∩SDS** (10 μM∩500 μM) and fluorescence spectra were recorded for a period of 3 days.

The rate of deterioration and release of spermine was found to be least after 5 hours in all the four food samples. It was found to be 25.16 mg/100 g, 28.68 mg/100 g, 35.11 mg/100 g and 19.56 mg/100 g for mushroom, cheese, chicken and mutton, respectively. When the storage period was extended to 18 hours, the spermine content increased to 30.97 mg/100 g, 33.67 mg/100 g, 38.59 mg/100 g and 23.19 mg/100 g for mushroom, cheese, chicken and mutton, respectively. Prolonging the storage periods to 27, 41, 50 and 65 hours, a small decrease in spermine content was noticed (Table 2). On storing the samples at 4 °C, no significant release of spermine was observed (Fig. 8).

Amongst literature references, entry 3 and ref. 14, the combination of a graphene quantum dots–cationic red dye donor–acceptor pair and cucurbit[7]uril reveals the lowest detection limits but is based on fluorescence quenching of the supramolecular complex at 535 nm on interaction with spermine (entry 3, Table 1). The self-assembly of a dye with CB[7] on interaction with SPD/SPM gives fluorescence enhancement in the NIR region (entry 4, Table 1) but has not been used for practical applications. The self-assemblies being reported here show fluorescence enhancement in the red (640 nm) and far-IR (720 nm) region and can find application in detection of spermine from serum, urine and food samples. Further, the smartphone relied RGB analysis facilitates the on-site determination of spermine in food samples.

3.9 Detection of spermine using a smartphone (RGB analysis)

In recent years, smartphone based analysis has provided a commercial and accurate method for on-site or real time determination of analytes in a portable manner.[36] The present study proposes a smartphone based determination of spermine *via* RGB profile analysis recorded by colour analyzer software installed in a Redmi Android smartphone (model number: Xiaomi K20 Pro). This software gives the RGB values of the images captured from different solutions (camera specifications: 48 MP, f/1.8, 26 mm wide). For capturing the
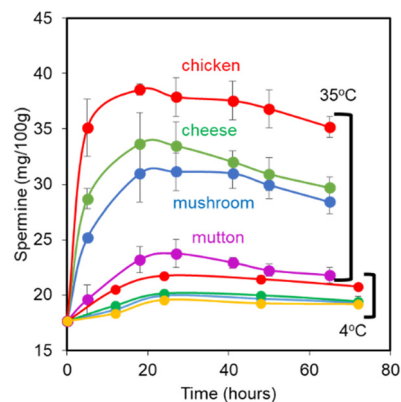

Fig. 8 Fluorescence point graph plot at 720 nm for the spermine content estimated in food samples (mushroom, cheese, chicken, mutton) stored at temperatures 35 and 4 °C at different time intervals using the **NIR-SPM∩SDS** ensemble in HEPES buffer.

images, the phone was kept at a distance of 25 cm from the sample. During the measurement, the distance between the UV light source and the sample was also kept constant. The colour analyzer software splits the sample's colour fluorescence image into red (R), green (G), and blue (B) channels. The desired analysis was conducted by adding various concentrations of spermine (0–80 μM) to the solution of **NIR-SPM** (10 μM)∩**SDS** (500 μM ensemble). The pictures of the prepared solutions were then taken using the smartphone and were separately analyzed by the software. It has been observed that as the concentration of spermine is increased, the intensity of the red colour is also increased as indicated by the red colour value given by the colour analyzer software and the change observed between 0–80 μM was linear with an R^2 value of 0.991 (Fig. 9). Further we have used the smartphone for the analysis of spermine content in the food samples as has been evaluated using the fluorescence technique. 5 grams of each food sample was taken in 10 ml of water. After 7 hours, 500 μl of water sample was added to the **NIR-SPM** (12 μM)∩**SDS** (600 μM) ensemble (2.5 ml) and was analyzed in terms of μM concentration in each water sample using the smartphone analysis linear calibration curve. These values were finally converted to mg/100 g in each sample. After 7 h, the amount of SPM released from mushroom, cheese, chicken, mutton was found to be 33.6 mg/100 g; 66.21 mg/100 g; 84.8 mg/100 g and 19.7 mg/100 g, respectively.

4. Conclusions

Thus, weakly fluorescent supramolecular assemblies of donor–π–acceptor dipods (**R-SPM**) (λ_{em} 640 nm) and (**NIR-SPM**) (λ_{em} 720 nm) exhibit 30–80 fold "turn-on" response towards spermine and can detect spermine at 22 nM (4.4 ppb) concentrations. AFM, DLS and zeta-potential studies conclusively delineate the formation of assemblies. The potential of these assemblies for real world applications like analysis of spermine from urine, human serum and food spoilage in the case of cheese, mushroom, chicken and

Table 2 The release of spermine at various time intervals in mushroom, cheese, chicken and mutton

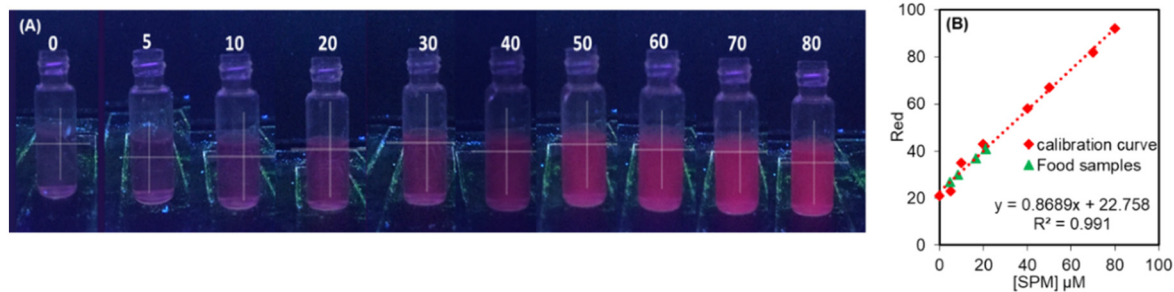| Sr. no.	Time (h)	[SPM] mushroom mg/100 g	[SPM] cheese mg/100 g	[SPM] chicken mg/100 g	[SPM] mutton mg/100 g
1	5	25.16	28.68	35.11	19.56
2	18	30.97	33.67	38.59	23.19
3	27	31.13	33.47	37.90	23.74
4	41	30.97	32.03	37.57	22.93
5	50	29.92	30.92	36.83	22.22
6	65	28.38	29.67	35.18	21.78

Fig. 9 (A) The apparent fluorescence colours of the **NIR∩SDS** (10 μM∩500 μM) solutions containing concentrations of spermine (0–80 μM) under 365 nm light; (B) the plot of the red component of images captured from solutions by the smartphone. The green points refer to the value of the red component from each food sample.

mutton has been demonstrated. The smartphone-relied RGB analysis speeds up the detection procedure, and also offers a new methodology for real-time analysis of spermine.

Human sample statement

The permission for the experiments with blood samples was provided by the institutional ethical committee, Guru Nanak Dev University, and in accordance with the declaration of Helsinki. Informed consents were obtained from all human subjects who participated in this study.

Conflicts of interest

There are no conflicts of interest to declare.

References

1 (*a*) H. Sanayama, K. Ito, S. Ookawara, T. Uemura, S. Imai, S. Kiryu, M. Iguchi, Y. Sakiyama, H. Sugawara, Y. Morishita, K. Tabei, K. Igarashi and K. Soda, *Biomedicines*, 2023, **11**, 746; (*b*) S. Saiki, Y. Sasazawa, M. Fujimaki, K. Kamagata, N. Kaga, H. Taka, Y. Li, S. Souma, T. Hatano, Y. Imamichi, N. Furuya, A. Mori, Y. Oji, S. I. Ueno, S. Nojiri, Y. Miura, T. Ueno, M. Funayama, S. Aoki and N. Hattori, *Ann. Neurol.*, 2019, **86**, 251–263; (*c*) A. Boffi, G. Favero, R. Federico, A. Macone, R. Antiochia, C. Tortolini, G. Sanzó and F. Mazzei, *Anal. Bioanal. Chem.*, 2015, **407**, 1131–1137.

2 S. A. Ibrahim, J. A. Zainulabdeen and H. M. Jasim, *Biomed. Pharmacol. J.*, 2018, **11**, 1389–1396.

3 (*a*) P. C. Kuo, C. W. Lien, J. Y. Mao, B. Unnikrishnan, H. T. Chang, H. J. Lin and C. C. Huang, *Anal. Chim. Acta*, 2018, **1009**, 89–97; (*b*) N. J. Martínez, M. G. Bejar, Y. M. Martínez, P. C. Falco and J. P. Prieto, *Anal. Chem.*, 2014, **86**, 1347–1351; (*c*) N. Tripathi, P. Singh, V. Luxami, D. Mahajan and S. Kumar, *Sens. Actuators, B*, 2018, **270**, 552–561; (*d*) R. Liu, Y. Jia, W. Cheng, J. Linga, L. Liu, K. Bi and Q. Li, *Talanta*, 2011, **83**, 751–756.

4 H. Deng, V. A. Bloomfield, J. M. Benevides and G. J. Jr, *Nucleic Acids Res.*, 2000, **28**, 3379–3385.

5 F. Madeo, M. A. Bauer, D. C. Gutierrez and G. Kroemer, *Autophagy*, 2019, **15**, 165–168.

6 S. M. Wortha, S. Frenzel, M. Bahls, M. Habes, K. Wittfeld, S. V. Auwera, R. Bülow, S. Zylla, N. Friedrich, M. Nauck, H. Völzke, H. J. Grabe, C. Schwarz and A. Flöel, *Alzheimer's Dementia*, 2023, **19**, 1832–1840.

7 E. W. Gerner, E. Bruckheimer and A. Cohen, *J. Biol. Chem.*, 2018, **293**, 18770–18778.

8 R. T. Tse, C. Y. P. Wong, P. K. F. Chiu and C. F. Ng, *Int. J. Mol. Sci.*, 2022, **23**, 1258.

9 R. A. Casero, T. M. Stewart and A. E. Pegg, *Nat. Rev. Cancer*, 2018, **18**, 681–695.

10 D. Doeun, M. Davaatseren and M. S. Chung, *Food Sci. Biotechnol.*, 2017, **26**, 1463–1474.

11 P. Song, L. Wu and W. Guan, *Nutrients*, 2015, **7**, 9872–9895.

12 M. Cantwell and C. Elliott, *J. Clin. Nutr. Diet.*, 2017, **3**, 27.

13 P. B. Tsafack and A. Tsopmo, *Heliyon*, 2022, **8**, 10456.

14 A. A. Bhosle, M. Banerjee, S. D. Hiremath, D. S. Sisodiya, V. G. Naik, N. Barooah, A. C. Bhasikuttan, A. Chattopadhyaya and A. Chatterjee, *J. Mater. Chem. B*, 2022, **10**, 8258–8273.

15 A. A. Bhosle, M. Banerjee, N. Barooah, A. C. Bhasikuttan, K. Kadu, S. R. Ramanan and A. Chatterjee, *J. Photochem. Photobiol., A*, 2022, **426**, 113770.

16 V. G. Naik, V. Kumar, A. C. Bhasikuttan, K. Kadu, S. Roy Ramanan, A. A. Bhosle, M. Banerjee and A. Chatterjee, *ACS Appl. Bio Mater.*, 2021, **4**, 1813–1822.

17 H. Tian, X. Yu, J. Yao, G. Gao, W. Wu and C. Yang, *Chem. Commun.*, 2021, **57**, 1806–1809.

18 N. N. Nghia, B. T. Huy, P. T. Phong, J. S. Han, D. H. Kwon and Y. Lee, *PLoS One*, 2021, **16**, 0251306.

19 S. Chopra, J. Singh, H. Kaur, A. Singh, N. Singh and N. Kaur, *Eur. J. Inorg. Chem.*, 2015, **2015**, 4437–4442.

20 K. Kumar, S. Kaur, S. Kaur, G. Bhargava, S. Kumar and P. Singh, *J. Mater. Chem. B*, 2019, **7**, 7218–7227.

21 P. Singh, P. Sharma, N. Sharma and S. Kaur, *Microchem. J.*, 2022, **183**, 108004.

22 S. K. Kailasa, M. L. Desai, S. H. Baek, L. M. T. Phan, T. P. Nguyen, R. Rafique and T. J. Park, *New J. Chem.*, 2019, **43**, 17069.

23 P. C. Kuo, C. W. Lien, J. Y. Mao, B. Unnikrishnan, H. T. Chang, H. J. Lin and C. C. Huang, *Anal. Chim. Acta*, 2018, **1009**, 89–97.

24 J. R. Bhamore, Z. V. P. Murthy and S. Kumar Kailasa, *J. Mol. Liq.*, 2019, **280**, 18–24.

25 K. A. Rawat, J. R. Bhamore, R. K. Singhal and S. K. Kailasa, *Biosens. Bioelectron.*, 2017, **88**, 71–77.

26 S. Chopra, J. Singh, H. Kaur, H. Singh, N. Singh and N. Kaur, *New J. Chem.*, 2015, **39**, 3507.

27 H. Jiang, X. Rao, L. Li and Z. Liu, *Analyst*, 2020, **145**, 7673.

28 Z. De Liu, H. Y. Zhu, H. X. Zhao and C. Z. Huang, *Talanta*, 2013, **106**, 255–260.

29 J. Wang, Q. Zhang, Z. D. Liu and C. Z. Huang, *Analyst*, 2012, **137**, 5565.

30 M. Barros, S. Ceballos, P. Arroyo, J. A. Sáez, M. Parra, S. Gil, A. M. Costero and P. Gaviña, *Chemosensors*, 2022, **10**, 8.

31 J. Huang, W. Ye, S. Zha, Y. Tao, M. Yang, K. Huang, J. Liu, Y. H. Fung, Y. Li, P. Li, L. Zhu and C. S. Lee, *J. Lumin.*, 2021, **232**, 117856.

32 M. Nakamura, T. Sanji and M. Tanaka, *Chem. – Eur. J.*, 2011, **17**, 5344–5349.

33 G. Jiang, W. Zhu, Q. Chen, X. Li, G. Zhang, Y. Li, X. Fan and J. Wang, *Sens. Actuators, B*, 2018, **261**, 602.

34 N. Meher and P. K. Iyer, *Angew. Chem., Int. Ed.*, 2018, **57**, 8488–8892.

35 J. Zeng, J. Wu, H. Chen and S. Ni, *International Journal of Agricultural Science and Food Technology*, 2021, **7**, 331–334.

36 (*a*) S. Banik, S. K. Melanthota, Arbaaz, J. M. Vaz, V. M. Kadambalithaya, I. Hussain, S. Dutta and N. Mazumder, *Anal. Bioanal. Chem.*, 2021, **413**, 2389–2406; (*b*) K. E. McCrackena and J. Y. Yoon, *Anal. Methods*, 2016, **8**, 6591–6601; (*c*) Pratibha, A. Kapoor, J. K. Rajput and A. Kumar, *Anal. Chem.*, 2022, **94**, 17685–17691.

37 P. Singh, L. S. Mittal, G. Bhargava and S. Kumar, *Chem. – Asian J.*, 2017, **12**, 890–899.

38 A. H. Malik, S. Hussain and P. K. Iyer, *Anal. Chem.*, 2016, **88**, 7358–7364.

39 S. A. Moayed, A. Bigdeli and M. R. H. Nezhad, *Food Chem.*, 2022, **384**, 132459.

40 R. R. Nair, S. Debnath, S. Das, P. Wakchaure, B. Ganguly and P. B. Chatterjee, *ACS Appl. Bio Mater.*, 2019, **2**, 2374–2387.